
LARGE-SCALE PORTFOLIO OPTIMIZATION USING PAULI CORRELATION ENCODING

Vicente P. Soloviev

Fujitsu Research of Europe Ltd.
Madrid, Spain

vicente.perezsoloviev@fujitsu.com

Michał Krompiec

Fujitsu Research of Europe Ltd.
Slough, UK

michal.krompiec@fujitsu.com

October 2025

ABSTRACT

Portfolio optimization is a cornerstone of financial decision-making, traditionally relying on classical algorithms to balance risk and return. Recent advances in quantum computing offer a promising alternative, leveraging quantum algorithms to efficiently explore complex solution spaces and potentially outperform classical methods in high-dimensional settings. However, conventional quantum approaches typically assume a one-to-one correspondence between qubits and variables (e.g. financial assets), which severely limits the applicability of gate-based quantum systems due to current hardware constraints. As a result, only quantum annealing-like methods have been used in realistic scenarios. In this work, we show how a gate-based variational quantum algorithm can be applied to a real-world portfolio optimization problem by assigning multiple variables per qubit, using the Pauli Correlation Encoding algorithm. Specifically, we address a problem involving over 250 variables, where the market graph representing a real stock market is iteratively partitioned into sub-portfolios of highly correlated assets. This approach enables improved scalability compared to traditional variational methods and opens new possibilities for quantum-enhanced financial applications.

Keywords Portfolio Optimization · Pauli Correlation Encoding · Variational Algorithm

1 Introduction

Portfolio optimization has become a trending problem in financial decision-making, which involves optimal allocation of capital among a set of financial assets to achieve specific investment objectives. It usually consists of maximizing expected return while minimizing the risk [Markowitz, 1952]. However, as real-world constraints and the dimensionality of financial markets increase, classical optimization approaches often encounter computational bottlenecks due to the complexity of the problem. Recent advances in quantum computing have opened new avenues for addressing such combinatorial optimization challenges [Abbas et al., 2024].

Recent gate-based approaches for portfolio optimization include Quantum Approximate Optimization Algorithm (QAOA) [Farhi et al., 2014, Kerenidis et al., 2019, Uotila et al., 2025, Huot et al., 2024, Stopfer and Wagner, 2025] and Variational Quantum Eigensolver [Peruzzo et al., 2014, Wang et al., 2025a,b]. However, the main limitation of these approaches is the scalability to real use cases. Specifically, the number of qubits required (n) increases linearly with the number of assets

(m), i.e., $\mathcal{O}(n)$, which quickly exceeds the capacity of current quantum devices as m grows. To mitigate this, recent research has explored circuit cutting, which partition large quantum circuits into smaller, more manageable subcircuits that can be executed independently and recombined classically [Soloviev et al., 2025]. Nevertheless, even with these advancements, the largest portfolio optimization problems addressed to date remain limited to fewer than $m = 100$ assets, underscoring the ongoing challenge of scaling gate-based quantum algorithms for practical financial optimization tasks.

In addition to gate-based quantum algorithms, alternative approaches such as quantum annealing and digital annealer [Sakuler et al., 2025, Phillipson and Bhatia, 2021] have been explored for portfolio optimization, particularly for large-scale and combinatorial instances. They both utilize specialized hardware or algorithms to mimic the annealing process and solve similar Quadratic Unconstrained Binary Optimization (QUBO) formulations at scale. These methods have demonstrated the ability to handle portfolio problems involving hundreds or even thousands of assets, offering a level of scalability that currently surpasses gate-based quantum devices. However,

despite their practical utility, neither quantum annealing nor digital annealing has yet exhibited a clear quantum advantage over state-of-the-art classical optimization algorithms Stopfer and Wagner [2025].

In this paper we use a recently developed qubit encoding Sciorilli et al. [2025] in which each of the qubits in the quantum system encodes more than one variable of the optimization problem. By using this encoding in combination with a variational approach we drastically reduce the required number of qubits, and solve a portfolio optimization problem over a market graph with more than $m = 250$ variables (number of stock assets). We show an extensive benchmarking against QAOA (for small instances) and a classical optimizer (for large instances), following an iterative bipartition strategy.

The article is structured as follows: Section 2 describes the main concepts regarding portfolio optimization and the qubit encoding used in the approach; Section 3 describes the followed methodology and results found; Section 4 rounds the paper off with some further conclusions and future research lines.

2 Background

2.1 Portfolio optimization

Portfolio optimization is a key component of contemporary quantitative finance, which focuses on allocating capital across a group of assets in order to strike the best possible balance between risk and projected return. Markowitz [1952] developed the traditional mean-variance paradigm, which represents a portfolio's expected return as the weighted sum of the returns of its individual assets:

$$\mu_p = \sum_{i=1}^N w_i \mu_i \quad (1)$$

where μ_p is the expected portfolio return, w_i is the weight of asset i in the portfolio, μ_i is the expected return of asset i , and N is the total number of assets.

Risk is typically quantified by the portfolio variance, which incorporates both the variances of individual assets and their pairwise correlations:

$$\sigma_p^2 = \sum_{i=1}^N \sum_{j=1}^N w_i w_j \sigma_{ij} \quad (2)$$

where σ_{ij} is the covariance between assets i and j . The covariance can be further expressed in terms of the correlation coefficient ρ_{ij} and standard deviations σ_i, σ_j :

$$\sigma_{ij} = \rho_{ij} \sigma_i \sigma_j \quad (3)$$

The correlation coefficient ρ_{ij} measures the linear relationship between the returns of assets i and j :

$$\rho_{ij} = \frac{\text{Cov}(r_i, r_j)}{\sigma_i \sigma_j} \quad (4)$$

where r_i and r_j are the returns of assets i and j , respectively.

In addition to the mean-variance framework, a widely used metric for evaluating portfolio performance is the Sharpe ratio, introduced by Sharpe (1966). The Sharpe ratio measures the risk-adjusted return of a portfolio by comparing its excess return over a risk-free rate to its standard deviation:

$$\text{Sharpe Ratio} = \frac{\mu_p - r_f}{\sigma_p} \quad (5)$$

where μ_p is the expected portfolio return, r_f is the risk-free rate, and σ_p is the standard deviation of portfolio returns. A higher Sharpe ratio indicates a more favorable risk-return trade-off, making it a key criterion in portfolio selection and optimization. Unlike raw return metrics, the Sharpe ratio accounts for volatility, thus enabling more robust comparisons across strategies with differing risk profiles.

This metric is particularly relevant in the context of this study, where multiple optimization strategies are benchmarked not only by their absolute returns but also by their ability to manage risk effectively. In subsequent sections, we use the Sharpe ratio to evaluate the performance of portfolios.

Several real-world limitations, including minimum/maximum position sizes, cardinality constraints, and transaction costs, affect portfolio optimization in practice. As a result, the problem is frequently non-convex and computationally difficult. In the last decades, several approaches directly address the graph representation of the stock market to design efficient portfolios. Thus, a market graph is constructed by representing the financial assets as nodes in the graph and the conditional relationships, such as ρ_{ij} or σ_{ij} , as edges.

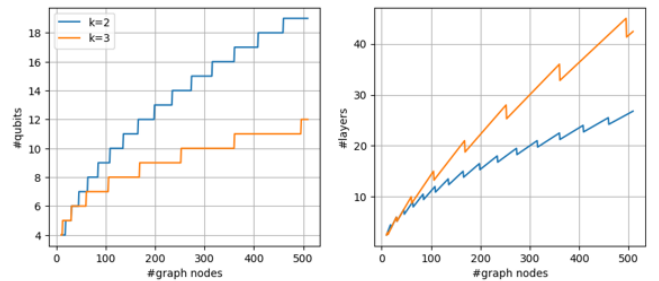


Figure 1: Number of qubits, and layers as a function of the number of variables in the problem to be solved

2.2 Pauli Correlation Encoding

Pauli Correlation Encoding (PCE) [Sciorilli et al., 2025] introduces a novel approach for embedding more than one optimization variable per qubit in the system. Specifically, the number of binary variables (m) using n qubits are encoded as $\mathcal{O}(n^k)$, where k is the order chosen by the user. This encoding

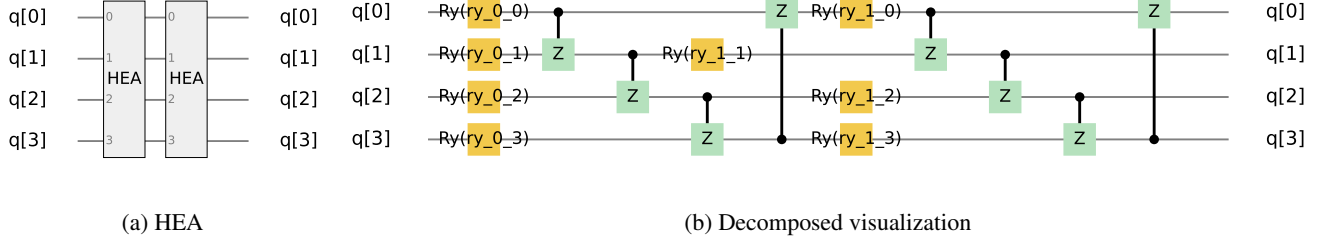


Figure 2: HEA built with a linear entangling structure and CZ gates, used in PCE strategy approach where $m = 10$, $n = 4$, $k = 2$ and $p = 2$.

is achieved by using a sign function over the Pauli-matrix correlations across multiple qubits (k). Thus, each binary variable is defined as:

$$x_i = \text{sgn}(\langle \Pi_i \rangle) \quad \forall i \in m, \quad (6)$$

where sgn is a sign function, and $\langle \Pi_i \rangle = \langle \Psi | \Pi_i | \Psi \rangle$ is the expectation value of Π_i , over a quantum system Ψ . The definition of the Pauli strings (Π_i) depends on the order (k) chosen by the user. The seminal paper suggests that a quadratic order will return better results when m is small, and cubic order will outperform the former for an increasing number of variables. Then, we define $\Pi^k = \{\Pi_1^k, \dots, \Pi_m^k\}$ where each Π_i^k is a permutation of either $X^k \otimes I^{n-k}$, $Y^k \otimes I^{n-k}$ or $Z^k \otimes I^{n-k}$, which are mutually commuting.

By using this encoding, the number of optimization variables improves upon the one-hot-encoding used in traditional approaches such as QAOA (equivalent to $k = 1$). Figure 1(left) shows the scaling of n as a function of m and k where $k = 3$ shows an improvement for larger m .

Another differentiating feature of this approach against other quantum variational approaches is that the quantum circuit used during the runtime is not dependent on the target problem. Then, the complexity of the original problem will not increase the depth of the circuit, as in QAOA, whose depth depends on the number of edges or quadratic terms in the problem. In this paper, we will use the Hardware Efficient Ansatz [Kandala et al., 2017] circuit. The required number of layers (p) is defined as $p = \lfloor m/n \rfloor$ (Figure 1(right)). Figure 2 shows a visual representation of the HEA where $m = 10$, $n = 4$, $k = 2$ and $p = 2$.

The variational approach consists in optimizing the parameters according to a cost function that reflect the optimization task to be solved. The seminal PCE paper Sciorilli et al. [2025] proposes the following function:

$$\mathcal{L} = \sum_{(i,j) \in E} w_{ij} \tanh(\alpha \langle \Pi_i \rangle) \tanh(\alpha \langle \Pi_j \rangle) + \mathcal{L}^{\text{reg}}, \quad (7)$$

where E is the number of edges in the original graph, α usually tuned to $\alpha = n^{\lfloor k/2 \rfloor}$, and \mathcal{L}^{reg} is a regularization term.

3 Method and results

3.1 Market graph representation

As explained in Section 2.1, a market graph is a representation of a real stock market. In this paper, we work with real data from the S&P 500 stock market¹ containing 5 years of data. Since we perform the benchmark for various sizes of the portfolio, the experiment with m assets will use the first m columns of the dataset. Thus, the results for bigger m will partially overlap with the results for smaller subsets of assets.

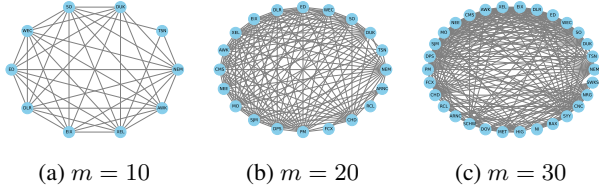


Figure 3: Market graph with m nodes where nodes represent stock assets.

The market graph \mathcal{G} assigns each asset to a node and contains an edge between nodes i and j only if their pairwise Pearson correlation (ρ_{ij}) is above a certain threshold λ , and no edge otherwise. It has been widely studied that an all-to-all graph connectivity in \mathcal{G} does not represent the real behavior of the stock market [Chmielewski et al., 2020, Namaki et al., 2011]. Thus,

$$w_{ij} = \begin{cases} 1 - |\rho_{ij}| & \text{if } |\rho_{ij}| > \lambda \\ \emptyset & \text{otherwise} \end{cases}, \quad (8)$$

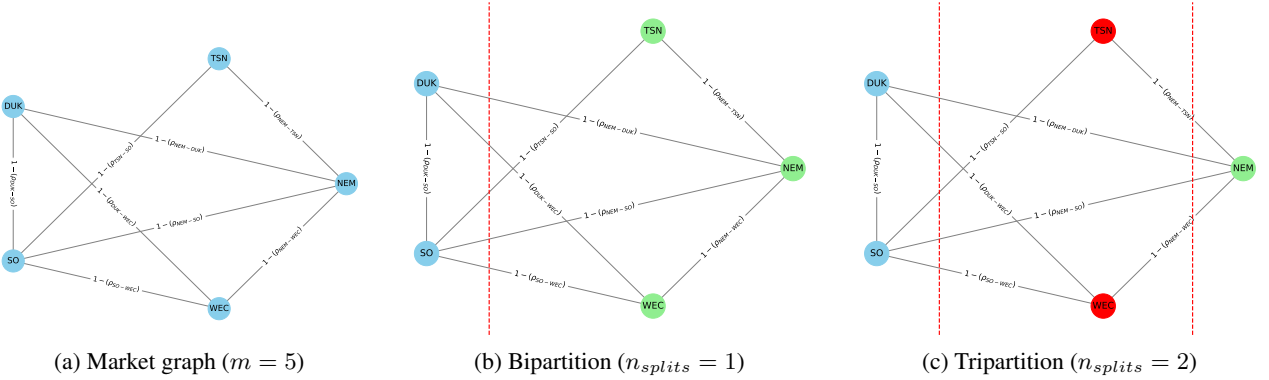
where $|\cdot|$ is the absolute value and \emptyset means that no edge is drawn.

The optimal choice of cuts over \mathcal{G} , will find the optimal portfolio for the desired strategy of investment. This graph-based approach has been traditionally exploited for portfolio diversification from the classical computation perspective for multiple purposes such as dynamic optimization [Arroyo et al., 2022], risk analysis [Ciciretti and Pallotta, 2024] and community detection [Zhao et al., 2021]; but also from the quantum

¹<https://www.kaggle.com/datasets/camnugent/sandp500>

# Nodes	# Edges	Density	Avg. Degree	Clustering Coeff.
10	39	0.867	7.80	0.95
20	137	0.721	13.7	0.92
30	230	0.528	15.3	0.70
50	714	0.560	28.0	0.77
100	3154	0.630	63.08	0.80
150	7606	0.680	101.4	0.82
200	14163	0.710	141.63	0.85
250	20948	0.660	166.91	0.83

Table 1: Market graph characteristics across different graph sizes

Figure 4: Iterative partition of the market graph (a) with $m = 5$ nodes, into two (b) and three (c) subgraphs by performing cuts over the representation. Cuts are represented with red dashed lines, and same color nodes represent correlated assets within the same cluster.

computing perspective for portfolio diversification [Acharya et al., 2025, Soloviev et al., 2025].

In this paper, our experiments show results for graphs sizes of $m \in \{10, 20, 30, 50, 100, 150, 200, 250\}$. Figure 3 shows the graph representations for $m \in \{10, 20, 30\}$ and Table 1 summarizes the structural characteristics of market graphs for the interest of visualization. For each graph size, the number of edges, graph density, average node degree, and average clustering coefficient are shown. These metrics provide insight into the connectivity and local structure of the graphs. As the number of nodes increases, both the average degree and the clustering coefficient tend to grow, indicating a denser and more interconnected topology. The density remains relatively stable across scales. While some works [Parekh, 2025, Stopfer and Wagner, 2025] state the efficiency of classical solvers for sparse graphs, our study focuses on dense market graphs (see as shown in table), where classical cut-finding becomes computationally demanding and quantum methods may offer practical advantages.

3.2 Bipartition strategy

Building upon the market graph \mathcal{G} introduced in the previous Section, we propose a recursive bipartitioning methodology aimed at decomposing the graph into a predefined number of subgraphs. The core principle of this approach is to iter-

atively split \mathcal{G} into two disjoint subsets by optimizing a cost function that reflects the structural dependencies among assets. Specifically, the algorithm seeks to maximize the number of cuts performed, thereby ensuring that each resulting subgraphs comprises assets that are highly correlated within each subgraph.

To formalize this, we define the following cut function:

$$\text{Cut}(\mathcal{G}, \mathbf{x}) = \sum_{v_i, v_j \in E} w_{ij} x_i (1 - x_j), \quad (9)$$

where $\mathbf{x} \in \{0, 1\}^m$ is a binary vector of length $m = |\mathcal{V}(\mathcal{G})|$. Each entry x_i denotes the assignment of asset i to one of the two subgraphs: $x_i = 0$ if asset i belongs to subgraph \mathcal{G}_0 , and $x_i = 1$ otherwise. The edge weights w_{ij} are defined following Equation 8.

By maximizing Equation 9, the algorithm encourages the separation of weakly connected components while preserving strong intra-subgraph connectivity. This results in partitions that are internally cohesive and externally sparse, which is a desirable outcome for our approach.

Algorithm 1 describes the proposed strategy, where by performing n_{splits} splits, $n_{splits} + 1$ subgraphs are generated. The algorithm iteratively calls `bipartition(\mathcal{G}_{aux} , measurement , k)` (line 22) over graph \mathcal{G}_{aux} from which two subsets of assets are returned.

Algorithm 1: Generate n Portfolio Partitions via PCE Bipartitioning**Input:** Number of splits n_{splits} , Graph \mathcal{G} , measurement, order k **Output:** Partition $(\mathcal{L}_1, \dots, \mathcal{L}_{n_{\text{splits}}+1})$

```

1 Initialize  $G_{\text{to\_split}} \leftarrow [\mathcal{G}]$ ;
2 Initialize  $L_{\text{labels}} \leftarrow [0]$ ;
3 Function bipartition( $\mathcal{G}$ ,  $\text{measurement}$ ,  $k$ ):
4    $\theta \leftarrow$  Initialize symbol map;
5    $n \leftarrow$  Find  $n$  such that  $m \leq 3 \binom{n}{k}$ ;
6    $p \leftarrow \lfloor m/n \rfloor$ ;
7    $\Psi(\theta) \leftarrow$  Prepare HEA circuit with  $n$  qubits and  $p$  layers;
8   Function  $f(\theta)$ :
9      $\Psi \leftarrow$  Set circuit parameters to  $\theta$ ;
10     $\Pi^k = \{\Pi_1^k, \dots, \Pi_m^k\} \leftarrow$  Compute  $\langle \Psi | \Pi_i | \Psi \rangle$  for all  $i \in [1, m]$  using  $\text{measurement}$ ;
11     $\mathbf{x} = [x_1, \dots, x_m] \leftarrow$  Compute binary representation (Eq. 6);
12    Compute loss function  $\mathcal{L}(\mathcal{G}, \Pi^k)$  (Eq. 7);
13    return  $(\mathcal{L}(\mathcal{G}, \Pi^k), \mathbf{x})$ 
14   $(\mathcal{L}_{\text{min}}, \mathbf{x}_{\text{min}}) \leftarrow$  minimize  $f$  using classical optimizer;
15   $S_1 \leftarrow \{i \mid \mathbf{x}_{\text{min}}[i] > 0\}$ ;
16   $S_2 \leftarrow \{i \mid \mathbf{x}_{\text{min}}[i] \leq 0\}$ ;
17  return  $(S_1, S_2)$ 
18
19 for  $i \leftarrow 1$  to  $n_{\text{splits}}$  do
20    $G_{\text{aux}} \leftarrow G_{\text{to\_split}}[0]$ ;
21   if  $|V(G_{\text{aux}})| > 1$  then
22      $S_1, S_2 \leftarrow$  bipartition( $G_{\text{aux}}$ ,  $\text{statevector}$ ,  $k$ );
23     Append  $G[S_1]$  and  $G[S_2]$  to  $G_{\text{to\_split}}$ ;
24     Append  $S_1$  and  $S_2$  to  $L_{\text{labels}}$ ;
25   else
26     Append  $G_{\text{to\_split}}[0]$  to  $G_{\text{to\_split}}$ ;
27     Append  $L_{\text{labels}}[0]$  to  $L_{\text{labels}}$ ;
28      $n_{\text{splits}} \leftarrow n_{\text{splits}} + 1$ ;
29   Remove first element from  $G_{\text{to\_split}}$ ;
30   Remove first element from  $L_{\text{labels}}$ ;
31 return  $L_{\text{labels}}$ 

```

The algorithm iteratively splits the subgraphs until the convergence criteria is met (line 19). In our experiments we use the `statevector` simulation as the measurement in the approach, although it is generalizable to other types of shot-based measurements, as suggested in Sciorilli et al. [2025] for PCE approach. The function `bipartition` (line 3) executes the PCE approach (Section 2.2) to solve the loss function (Equation 9) and maps the resultant binary string into two subgraphs. This function internally computes the required number of qubits (line 5) and corresponding number of layers (line 6) for the HEA circuit (line 7). A classical optimizer is run to optimally tune the parameters (line 14). In this paper, the COBYLA optimizer [Gomez and Hennart, 2013] was used.

Figure 4 shows a toy example of the partition approach where a real market graph with $m = 5$ nodes (a) is split $n_{\text{splits}} = 1$ (b), and $n_{\text{splits}} = 2$ (c) times, respectively. Same color nodes represent highly correlated nodes within the same cluster of assets.

The outcome of Algorithm 1 is a collection of $n_{\text{splits}} + 1$ disjoint clusters, each comprising a subset of highly correlated assets. These clusters, denoted as $\{L_1, L_2, \dots, L_{n_{\text{splits}}+1}\}$, serve as the foundation for constructing a diversified portfolio. To ensure that the portfolio captures the most promising investment opportunities within each cluster, we select a single representative asset from each group according to its historical performance.

Let $L_i = [L_i^1, \dots, L_i^{|L_i|}]$ denote the set of assets in cluster L_i , where $|L_i|$ is the cardinality of the cluster. For each asset L_i^j in the cluster, we compute its return μ_i^j using a predefined return function (see Equation 1). This yields a return vector:

$$\boldsymbol{\mu}_i = [\mu_i^1, \dots, \mu_i^{|L_i|}],$$

which encapsulates the performance of all assets within cluster L_i . The representative asset r_i for cluster L_i is then selected as:

$$r_i = \arg \max_{j \in \{1, \dots, |L_i|\}} \mu_i^j,$$

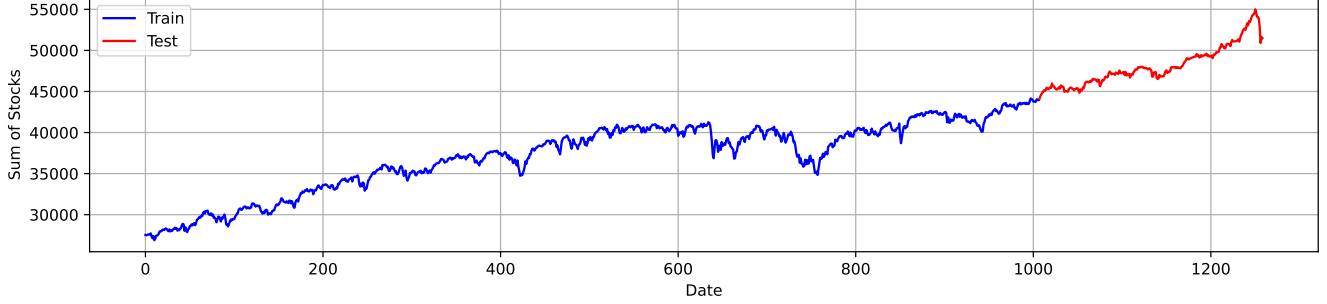


Figure 5: Aggregate of stock values in S&P 500 stock market along time. Blue and red parts represent training and testing fractions of the dataframe, respectively.

i.e., the asset with the highest return within its respective cluster. This selection criterion ensures that the final portfolio is composed of top-performing assets from structurally coherent groups, thereby balancing diversification with return optimization. We are aware here that other approaches have been used in the literature such as analyzing the sign of the pairwise correlation (4) among the assets within the same cluster L_i [Aref and Wilson, 2019; Harary et al., 2002].

The resulting portfolio, composed of $r = \{r_1, r_2, \dots, r_{n_{\text{splits}}+1}\}$, is expected to exhibit reduced internal redundancy due to the high intra-cluster correlation and enhanced overall performance due to the return-based selection mechanism.

3.3 Results

This section presents the experimental results obtained by applying the methodology outlined in Section 3.2 to the problem instances described in Section 3.1.

The dataset was partitioned into training and testing subsets, comprising 80% and 20% of the original data, respectively. The partitioning strategy was applied to the training set to identify a subset r of representative assets. The performance of the selected assets was subsequently evaluated on the testing set. Figure 5 illustrates the temporal evolution of the aggregate value of all assets in the dataset, providing an overview of the dataset's dynamics over time, where blue and red parts represent the training and test fractions, respectively.

As described previously, the iterative partitioning procedure recursively divides a subset of assets into two distinct subsets at each iteration. The dendrogram presented in Figure 6 visually captures the hierarchical structure resulting from the algorithm outlined in Algorithm 1. Each leaf node in the dendrogram corresponds to a group of highly correlated assets, denoted as L_i , for the case where $m = 50$. For clarity, individual assets have been anonymized and represented by numerical identifiers.

The vertical axis of the dendrogram reflects the depth of the recursive partitioning process, effectively mapping the sequence of iterations. Notably, the dendrogram reveals that the cardinality of the leaf-level groups L_i remains relatively balanced

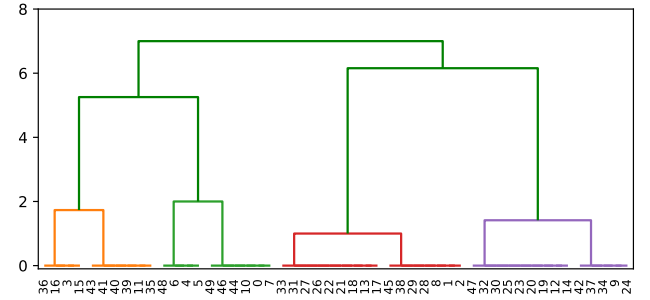


Figure 6: Dendrogram for $m = 50$, where each number in x-axis corresponds to a different stock company.

across the entire set, a structural property that persists consistently across all tested values of m . This observation suggests that the partitioning algorithm tends to produce evenly sized clusters.

In this study, we assess the performance of our proposed method across different problem instances, with sizes ranging from $m = 10$ to $m = 250$, as summarized in Table 1. To benchmark our approach against established optimization techniques, we consider two representative algorithms: QAOA, serving as a quantum method, and Estimation of Distribution Algorithms (EDAs), representing classical heuristics. QAOA is configured with $p = 5$ layers and applied exclusively to the smallest instance ($m = 10$), where the use of one-hot encoding within the partitioning framework remains computationally feasible. For larger instances ($m \geq 10$), EDAs are employed due to their scalability and adaptability to high-dimensional combinatorial spaces.

To ensure fair comparison across varying problem sizes, the number of recursive splits in the partitioning process is tuned according to instance size: specifically, $r_{\text{splits}} = 2, 4, 6, 9$ for $m < 100$, and $r_{\text{splits}} = (m/10) - 1$ for $m \geq 100$.

Figure 7 presents the benchmarking results, where QAOA ($p = 5$), PCE ($k = 3$), and EDA are depicted as red, orange, and green lines, respectively. Each algorithm executes the procedure described in Algorithm 1, using historical data from the training set to identify an optimal subset of representative

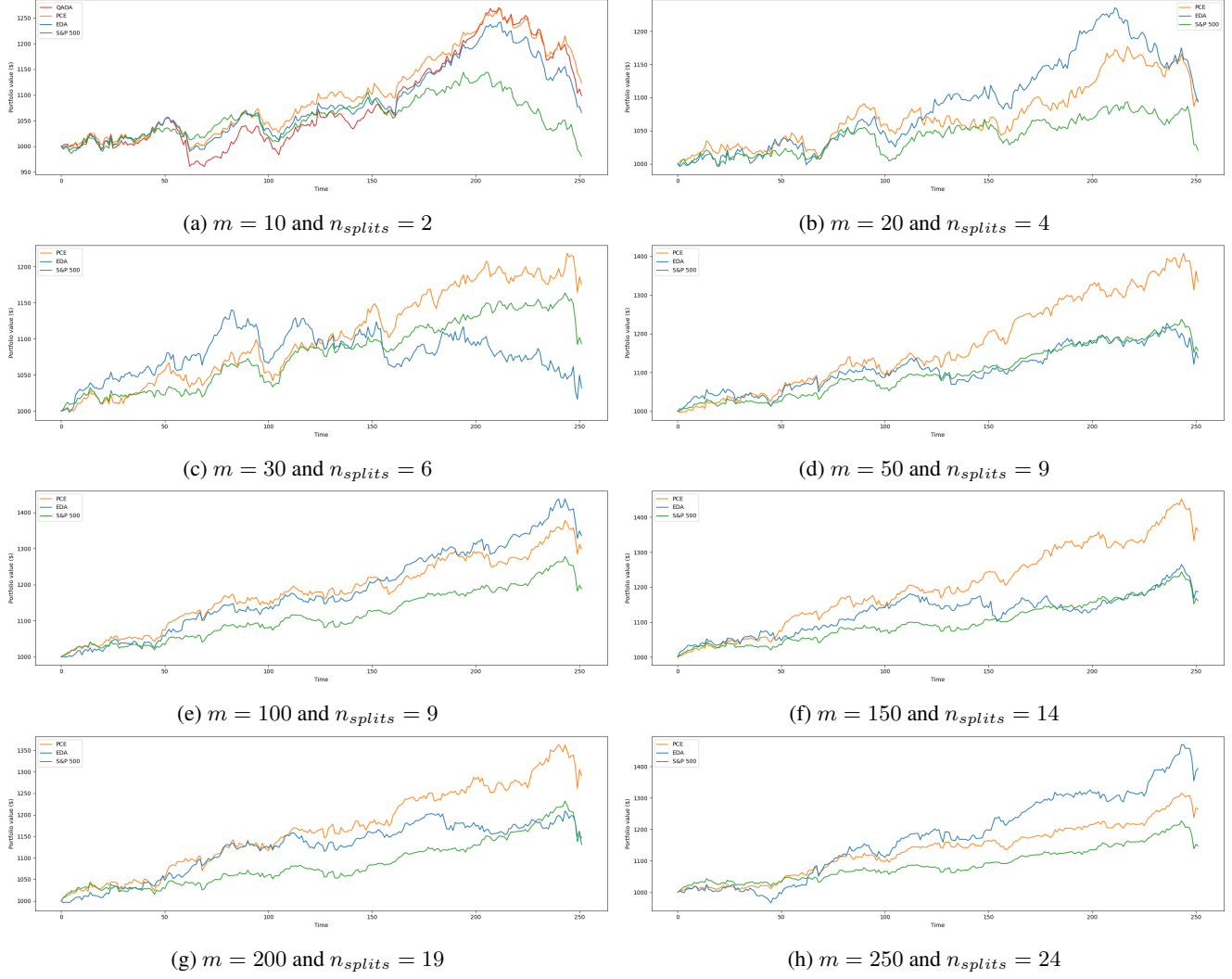


Figure 7: Comparison between money invested in S&P 500 stock market against the portfolio optimization strategy proposed.

assets r . The resulting portfolios are then evaluated on the test dataset, and their performance is visualized in the corresponding subplots. The figure illustrates the evolution of an initial investment of \$1000 over time, following the portfolio strategy derived from each optimizer, and compares it against the baseline performance of the full set of m assets without optimization.

The performance for $m = 10$ for QAOA and PCE is very similar in terms of the selection of assets. However, since QAOA is limited by the qubit encoding used, the problem instances tested might not be enough to conclude the performance of the approach. Table 2 reports the gate counts required by QAOA and PCE algorithms across a range of graph sizes, characterized by the number of nodes and edges. The QAOA gate counts are shown for two circuit depths, $p = 1$ and $p = 2$, while PCE shows order $k = 2$ and $k = 3$. As expected, the gate complexity for QAOA increases significantly with both the number of nodes and the circuit depth, reflecting the quadratic scaling of entangling operations in dense graphs.

For instance, QAOA with $p = 2$ requires over 42,000 gates for a graph with 250 nodes and nearly 21,000 edges. In contrast, PCE exhibits a much more modest growth in gate count, remaining under 750 gates even for the largest instance tested. This highlights the scalability advantage of PCE over QAOA, particularly for large problem instances where quantum resource constraints are prohibitive. Since $p = 5$ has been chosen for this problem instance, the scalability of QAOA is limited by the depth and number of qubits used.

For greater number of nodes $m \geq 10$, it is observed that the proposed strategy always outperforms the baseline for all the tested cases, regardless of the optimization procedure used. PCE shows the most robust and stable growth trajectory across all problem sizes. Its portfolio value steadily increases over time, often maintaining a clear lead over both EDA and the S&P 500. This suggests that PCE is effective at identifying representative assets that contribute to long-term portfolio growth. EDA, while also outperforming the baseline, exhibits greater volatility. It occasionally reaches higher peaks than

# Nodes	# Edges	QAOA ($p = 1$)	QAOA ($p = 2$)	PCE ($k = 2$)	PCE ($k = 3$)
10	39	59	108	25	25
20	137	177	334	61	61
30	230	290	550	91	91
50	714	814	1578	148	145
100	3154	3354	6608	298	295
150	7606	7906	15662	430	433
200	14163	14563	28926	586	595
250	20948	21448	42646	715	730

Table 2: Gate counts for QAOA (built with CZ) and PCE across graph sizes.

PCE ($m = 100$ and $m = 250$) but also experiences sharper drawdowns. This behavior indicates that while EDA can capture short-term opportunities, it may be more sensitive to market fluctuations or local optima in the asset selection process. The iterative behavior exhibited by the EDA reveals a distinct partitioning strategy, wherein a small number of nodes are incrementally separated from the main graph structure during each iteration. This contrasts with PCE, which consistently performs more balanced splits, typically dividing the graph into two subsets of comparable size. Such divergence in partitioning dynamics reflects fundamental differences in the underlying heuristics of each method and may influence the granularity and stability of r found.

Since the original market graph \mathcal{G} encodes pairwise Pearson correlations among stock assets, the optimization strategy initially focuses on structural properties rather than asset returns. Consequently, the selection of representative assets r is performed over the decision made in the graph. To evaluate the effectiveness of the selected representatives, Figure 8 presents a comparative analysis of the Sharpe ratio (Equation 5) for the PCE strategy and the baseline, shown as orange and blue bars, respectively, across both training and test datasets.

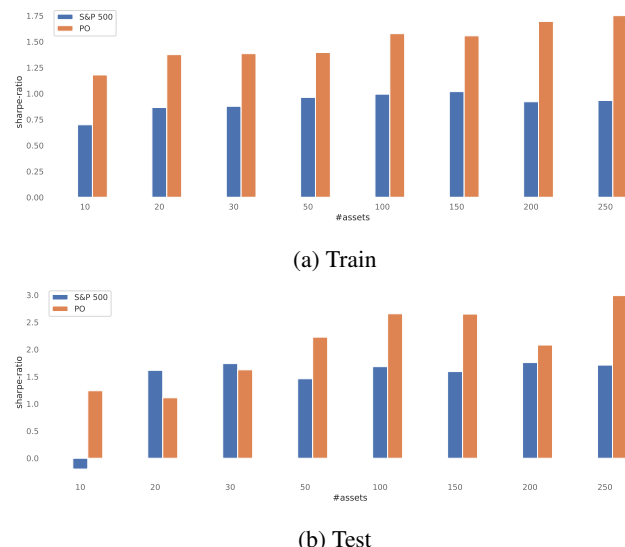


Figure 8: Sharpe-ratio comparison

Figure 8a shows that the PCE approach successfully identifies a subset r that yields a higher Sharpe ratio than the baseline, indicating superior risk-adjusted performance. This trend is consistent in the test dataset, as shown in Figure 8b, where PCE continues to outperform the baseline in most experiments. These results suggest that the proposed strategy effectively balances return maximization and risk minimization, as captured by the Sharpe ratio, despite its initial reliance on correlation structure rather than direct return information.

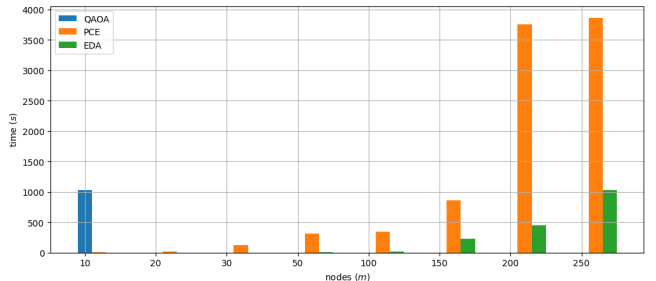


Figure 9: Times comparison (algorithm execution for single optimization problem)

To assess the computational efficiency of the proposed methods, Figure 9 shows a runtime analysis for a single iteration of Algorithm 1 with $n_{\text{splits}} = 1$. Figure 9 presents the runtime as a function of the number of nodes (m) involved in the optimization. As illustrated, QAOA exhibits the highest computational cost, with its runtime for $m = 10$ comparable to that of the PCE approach for $m = 150$. Notably, PCE is capable of solving instances with $m \geq 200$ in approximately one hour, indicating its practical viability for real-world applications. Note that statevector simulation was used for these experiments, and this runtime may decrease if a different measurement strategy or a real quantum device were used. Although the classical heuristic (EDA) generally requires less computational effort, its runtime may vary depending on the configuration of its hyperparameters.

4 Conclusions

In this work, we proposed a graph-based portfolio optimization strategy that iteratively bipartitions a market graph representing the S&P 500, where each node corresponds to a stock

asset and edges encode pairwise Pearson correlations. From each identified group of correlated assets, a representative is selected to construct an optimized portfolio. Traditional quantum gate-based models such as QAOA face scalability limitations due to one-hot encoding, which maps each asset to a separate qubit. To address this, we propose the usage of PCE method, enabling the representation of multiple optimization variables per qubit.

Our results demonstrate that instances involving more than $m > 250$ assets can be solved within approximately one hour using a statevector simulator, surpassing the scalability constraints of conventional quantum approaches. The proposed strategy effectively balances return maximization and risk minimization, as evidenced by superior Sharpe ratio performance compared to baseline methods. Although this study scales up to $m = 250$ and $n = 9$, the approach is designed to potentially accommodate the full S&P 500 stock market or larger asset sets at a cost of increasing the number of qubits n .

While the current implementation of PCE utilizes a Hardware-Efficient Ansatz, future work include the exploration of alternative quantum circuit architectures tailored to this problem. Additionally, further research will investigate enhanced methods for selecting representative assets from each correlated group to improve portfolio construction. Finally, we also propose the analysis of quantum noise resilience as a further analysis.

Acknowledgments

The authors would like to express their sincere gratitude to Bibhas Adhikari from Fujitsu Research of America for reviewing the paper and providing valuable feedback.

References

Harry Markowitz. Portfolio selection. *The Journal of Finance*, 7(1):77–91, 1952. doi: 10.1111/j.1540-6261.1952.tb01525.x.

Amira Abbas, Andris Ambainis, Brandon Augustino, Andreas Bärtschi, Harry Buhrman, Carleton Coffrin, Giorgio Corstiana, Vedran Dunjko, Daniel J Egger, Bruce G Elmegreen, et al. Challenges and opportunities in quantum optimization. *Nature Reviews Physics*, pages 1–18, 2024.

Edward Farhi, Jeffrey Goldstone, and Sam Gutmann. A quantum approximate optimization algorithm. *arXiv preprint arXiv:1411.4028*, 2014.

Iordanis Kerenidis, Anupam Prakash, and Dániel Szilágyi. Quantum algorithms for portfolio optimization. In *Proceedings of the 1st ACM Conference on Advances in Financial Technologies*, pages 147–155, 2019.

Valter Uotila, Julia Ripatti, and Bo Zhao. Higher-order portfolio optimization with quantum approximate optimization algorithm. *arXiv preprint arXiv:2509.01496*, 2025.

Chansreynich Huot, Kimleang Kea, Tae-Kyung Kim, and Yougsun Han. Enhancing knapsack-based financial portfolio optimization using quantum approximate optimization algorithm. *IEEE Access*, 2024.

Eric Stopfer and Friedrich Wagner. Quantum portfolio optimization: An extensive benchmark. *arXiv preprint arXiv:2509.17876*, 2025.

Alberto Peruzzo, Jarrod McClean, Peter Shadbolt, Man-Hong Yung, Xiao-Qi Zhou, Peter J Love, Alán Aspuru-Guzik, and Jeremy L O’brien. A variational eigenvalue solver on a photonic quantum processor. *Nature communications*, 5(1):4213, 2014.

Shengbin Wang, Peng Wang, Guihui Li, Shubin Zhao, Dongyi Zhao, Jing Wang, Yuan Fang, Menghan Dou, Yongjian Gu, Yu-Chun Wu, et al. Variational quantum eigensolver with linear depth problem-inspired ansatz for solving portfolio optimization in finance. *Science China Information Sciences*, 68(8):1–11, 2025a.

Anbang Wang, Zhonggang Lv, Zhenyuan Ma, Dunbo Cai, and Zhihong Zhang. Achieving high-quality portfolio optimization with the variational quantum eigensolver. *arXiv preprint arXiv:2508.18625*, 2025b.

Vicente P Soloviev, Antonio Márquez Romero, Josh Kirsopp, and Michal Krompiec. Scaling portfolio diversification with quantum circuit cutting techniques. *arXiv preprint arXiv:2506.08947*, 2025.

Wolfgang Sakuler, Johannes M Oberreuter, Riccardo Aiolfi, Luca Asproni, Branislav Roman, and Jürgen Schiefer. A real-world test of portfolio optimization with quantum annealing. *Quantum Machine Intelligence*, 7(1):1–22, 2025.

Frank Phillipson and Harshil Singh Bhatia. Portfolio optimisation using the d-wave quantum annealer. In *International Conference on Computational Science*, pages 45–59. Springer, 2021.

Marco Sciorilli, Lucas Borges, Taylor L Patti, Diego García-Martín, Giancarlo Camilo, Anima Anandkumar, and Leandro Aolita. Towards large-scale quantum optimization solvers with few qubits. *Nature Communications*, 16(1):476, 2025.

Abhinav Kandala, Antonio Mezzacapo, Kristan Temme, Maika Takita, Markus Brink, Jerry M Chow, and Jay M Gambetta. Hardware-efficient variational quantum eigensolver for small molecules and quantum magnets. *nature*, 549(7671):242–246, 2017.

Lukasz Chmielewski, Rafina Amin, Anak Wannaphaschayi-ong, and Xingquan Zhu. Network analysis of technology stocks using market correlation. In *2020 IEEE International Conference on Knowledge Graph (ICKG)*, pages 267–274. IEEE, 2020.

Ali Namaki, Amir H Shirazi, R Raei, and GR Jafari. Network analysis of a financial market based on genuine correlation and threshold method. *Physica A: Statistical Mechanics and its Applications*, 390(21-22):3835–3841, 2011.

Alvaro Arroyo, Bruno Scalzo, Ljubiša Stanković, and Danilo P Mandic. Dynamic portfolio cuts: A spectral approach to graph-theoretic diversification. In *ICASSP 2022-2022 IEEE International Conference on Acoustics, Speech and Signal Processing (ICASSP)*, pages 5468–5472. IEEE, 2022.

Vito Ciciretti and Alberto Pallotta. Network risk parity: graph theory-based portfolio construction. *Journal of asset management*, 25(2):136–146, 2024.

Longfeng Zhao, Chao Wang, Gang-Jin Wang, H Eugene Stanley, and Lin Chen. Community detection and portfolio optimization. *arXiv preprint arXiv:2112.13383*, 2021.

Atithi Acharya, Romina Yalovetzky, Pierre Minssen, Shouvanik Chakrabarti, Ruslan Shaydulin, Rudy Raymond, Yue Sun, Dylan Herman, Ruben S Andrist, Grant Salton, et al. Decomposition pipeline for large-scale portfolio optimization with applications to near-term quantum computing. *Physical Review Research*, 7(2):023142, 2025.

Ojas Parekh. No quantum advantage in decoded quantum interferometry for maxcut. *arXiv preprint arXiv:2509.19966*, 2025.

Susana Gomez and Jean-Pierre Hennart. *Advances in optimization and numerical analysis*, volume 275. Springer Science & Business Media, 2013.

Samin Aref and Mark C Wilson. Balance and frustration in signed networks. *Journal of Complex Networks*, 7(2):163–189, 2019.

Frank Harary, Meng-Hiot Lim, and Donald C Wunsch. Signed graphs for portfolio analysis in risk management. *IMA Journal of management mathematics*, 13(3):201–210, 2002.